RSC Advances

PAPER

View Article Online
View Journal | View Issue

Cite this: *RSC Adv.*, 2021, **11**, 18984

5FU encapsulated polyglycerol sebacate nanoparticles as anti-cancer drug carriers†

Divya Sivanesan,[a] Rama S. Verma *[a] and Edamana Prasad *[b]

The majority of anti-cancer drugs fail to reach clinical trials due to their low water solubility. A biocompatible drug delivery system that encapsulates and efficiently delivers hydrophobic drugs to the target site is the need of the hour. This study addresses the issue by focusing on a polymeric polyglycerol sebacate (PGS) nanoparticles loaded with 5-fluorouracil (5FU), a primary line chemotherapy drug for many types of cancers. The generated nanoparticle (PGS-NP) was biocompatible and had minimal cytotoxicity against the MDA-MB-231 and A549 cell lines, even at a high concentration of 100 μg mL^{-1}. The cell viability post treatment with PGS nanoparticles encapsulated with 5FU (PGS-5FU) decreased to as low as around 40% whereas, in the case of treatment with 5FU, the viability percentage increased. The nanoparticles also showed controlled drug release when encapsulated with 5FU. This striking observation suggested that these nanoparticles can improve the efficacy of drug delivery to tumor sites. Apoptosis assay and caspase-3 activity quantification supported these data wherein PGS-5FU treatment showed almost three times caspase-3 activity as compared to control cells. Additionally, throughout all the experiments, MDA-MB-231 cells were more sensitive to PGS-5FU than A549 cells, indicating that these nanoparticles are ideal for breast cancer treatment. In summary, 5FU encapsulated PGS nanoparticles are a potential drug carrier to deliver 5FU efficiently to cancer cells.

Received 4th March 2021
Accepted 10th May 2021

DOI: 10.1039/d1ra01722e

rsc.li/rsc-advances

1. Introduction

Cancer is the second leading death-causing disease according to the WHO.[1] The different types of cancer account for almost 10 million deaths per year.[2] Breast cancer is currently diagnosed in 1 out of 4 women globally,[3] and metastasis of this cancer is as high as 30%.[4] Similarly, the number of lung cancer cases reported in 2020 alone was 2.2 million[5] worldwide with the highest death rate of all cancer types. Whichever type of cancer is detected, the care and treatment given to patients include chemotherapy, radiotherapy or surgery or a combination.[6] Depending upon the stage and location of the tumor, the chemotherapy regime can include anti-cancer drugs such as 5-fluorouracil (5FU)[7–10] and paclitaxel.[11] Many of these drugs are hydrophobic with solubility and biocompatibility issues. This has hindered the drug development process over many decades. One of the solutions is to discover a vehicle for delivery of the drugs precisely to the site with high biocompatibility and bioavailability. This could also avoid relapse by improving the efficiency of the current therapy given to patients.

The recent trend in drug delivery systems has shifted towards nanomedicines like polymeric nanoparticles, liposomes, and micelles.[12] Organic and inorganic nanoparticles are gaining interest and as many as 25 have been approved by the FDA, and nearly 75 nanomedicines are currently in clinical trials.[13] The major advantages of nanoparticles are an improved bioavailability owing to their enhanced aqueous solubility and increased half-life.[14,15] As most cancer drugs have poor solubility, giving them as injections is challenging and tablet formulation can also be difficult.[16,17] By encapsulating these drugs within nanoparticles, a topical therapy can be refined.

Polymeric nanoparticles have been gaining attention due to their small particle size and their ability to protect encapsulated drugs from the biological environment with improved therapeutic indices. Regarding polymers used to synthesize nanoparticles, polyglycerol sebacate (PGS)[18–20] that is widely used as a scaffold in tissue engineering is less studied in the field of nanomedicines. The monomers that produce this polymer *via* polycondensation, glycerol and sebacic acid, are both FDA approved and biocompatible. This polymer has utility as a scaffold or patch due to its high tensile strength and elastomeric property.[21] By tweaking the molar ratios of the monomers, we can synthesize polymeric PGS as a gel that can then be made into nanoparticles (NPs)[22,23] using the solvent displacement method.[24] This has not been particularly well explored and very few studies have reported the application of PGS as a drug delivery system to treat cancer.

Here, in this study, PGS nanoparticles (PGS-NPs) are synthesized, characterized, and encapsulated with 5FU (PGS-

[a]*Department of Biotechnology, Indian Institute of Technology Madras, Chennai-600036, India. E-mail: vermars@iitm.ac.in*

[b]*Department of Chemistry, Indian Institute of Technology Madras, Chennai-600036, India. E-mail: pre@iitm.ac.in*

† Electronic supplementary information (ESI) available. See DOI: 10.1039/d1ra01722e

5FU), a common drug used in the treatment of breast cancer and whose derivates are currently being studied for targeted therapy against lung cancer. PGS-NPs had sizes within the range of 200–300 nm, and 5FU encapsulation did not vary the size much. These PGS nanoparticles also showed minimal cytotoxicity toward cancer cells, indicating their high biocompatibility. When loaded with 5FU, the cytotoxicity of these NPs increased significantly and over a long period of 48 h, the percentage of viable cells continued to decrease, showing a controlled drug release. This is one of the first studies reporting PGS nanoparticles encapsulated with 5FU as a drug delivery system for the treatment of breast cancer and lung cancer. When studying the effects of these drug-loaded NPs, it is evident that they provide an efficient way of delivering hydrophobic anti-cancer drugs to tumor sites.

2. Experimental section

2.1. Materials and methods

The chemicals and reagents were purchased from Sigma-Aldrich Chemical Co. Sebacic acid (cat. no. 283258) and glycerol (cat. no. G5516) were purchased from Sigma-Aldrich Chemical Co. 5-Fluorouracil (5FU), Tween 80, MTT (3-(4,5-dimethylthiazol-2-yl)-2,5-diphenyltetrazolium bromide), rhodamine B and other chemicals used for this study were obtained from Sisco Research Laboratories Pvt. Ltd. NMR spectra were recorded using a Bruker ADVANCE III 500 MHz spectrometer with DMSO-d_6 as the solvent. FTIR spectra were recorded using a Jasco FTIR-4100 instrument equipped with an ATR accessory. UV-visible spectra were collected using a PerkinElmer spectrophotometer. Thermogravimetric analysis (TGA) was performed under a nitrogen atmosphere with a heating rate of 10 °C min^{-1} using a TGA Q-50 thermogravimetric analyzer. Dynamic light scattering (DLS) was performed using a Malvern Instruments Zetasizer nano ZS90. Powder X-ray diffraction (XRD) was performed using a D8 Advance (Bruker). Scanning electron microscopy (SEM) was used to take images of the nanoparticles and the SEM instrument was bought from Thermo Fisher Scientific (Apreo S). The colorimetric caspase-3 assay was purchased from Takara Bio. Annexin V-FITC and propidium iodide were obtained from BD Biosciences. The primary and secondary-HRP conjugated antibodies used for western blot analysis were obtained from Cell Signaling Technology.

2.2. Maintenance of cell lines

Human non-small-cell lung cancer cell line A549 and human breast cancer cell line MDA-MB-231 were procured from the National Centre for Cell Sciences (NCCS), Pune, Maharashtra, India. They were cultured in DMEM (Gibco, Grand Island, U.S.A.) supplemented with 10% fetal bovine serum (FBS) (Gibco, Grand Island, U.S.A.) with 1× penicillin–streptomycin (Gibco, Grand Island, U.S.A.) with 5% CO_2 at 37 °C in a humified incubator.

2.3. Synthesis of the polyglycerol sebacate pre-polymer

The polyglycerol sebacate polymer was synthesized using a previously reported procedure.[25] Equimolar amounts of glycerol and sebacic acid were taken and kept in an oil bath at 120 °C for 24 h under a nitrogen atmosphere with constant magnetic stirring. After 24 h, a sticky-gel polymer formed, which was dissolved in ethanol and purified using distilled water and a 10 000 Da dialysis bag. This solution was freeze-dried and stored at room temperature. FTIR (PGS) (cm^{-1}): 3443, 2926, 2854, 1733, 1410, 1180, 936; ^{1}H NMR (PGS) (500 MHz) δ/ppm: 1.24 (s, –CH_2–), 1.55 (d, –CH_2-CH_2O(CO)–), 2.27 (m, –CH_2O(CO)–), 3.6–4.1 (m, OHCH_2CHO–), 4.2–4.35 (m, –OCH_2CHO–), 4.95 (2-acylglyceride), 5.09 (1,2-diacylglyceride), 5.26 (1,2,3-triacylglyceride).

2.4. Preparation of PGS nanoparticles

The nanoparticles were generated using the solvent displacement method. Different amounts of PGS were taken and dissolved in 1 mL of ethanol to obtain different concentrations of the nanoparticles (5 mg mL^{-1}, 10 mg mL^{-1}, 20 mg mL^{-1}, and 25 mg mL^{-1}).[22] This solution was added dropwise to 10 mL of distilled water slowly and 100 μL of Tween 80 was also added. The solution was kept under constant stirring with sonication at 60 °C. It was then centrifuged at a high speed of 12 000*g* for 10 min and the supernatant was discarded. The pellet was washed with phosphate buffer saline (PBS) twice at high speed for 5 min. This pellet was then freeze-dried and weighed for further experiments.

2.5. Encapsulation of 5FU within the nanoparticles

The 5FU drug and PGS nanoparticles were taken in different ratios (1 : 1, 1 : 2, 1 : 2.5, 1 : 4, and 1 : 5) to optimize the loading efficiency of the 5FU loaded nanoparticles. 5FU was dissolved in 1 mL of DMSO and this solution was added to 9 mL of distilled water (1 : 10) containing 250 mg of PGS (25 mg mL^{-1}).[26] This mixture was left stirring overnight. Then, the solution was centrifuged at a high speed of 12 000*g* for 10 min and the supernatant was discarded. The pellet was washed with phosphate buffer saline (PBS) at high speed for 5 min and the supernatant was taken for UV-vis spectral measurement at 508 nm to calculate the amount of encapsulated 5FU. After washing with PBS, the pellet was lyophilized and weighed. The loading efficiency[27] was calculated using the following formula:

$$\text{Loading efficiency}\% = \frac{(\text{Total amount of 5FU}) - (\text{amount of 5FU washed}) \times 100}{\text{Total amount of 5FU}}$$

2.6. Characterization of 5FU loaded PGS nanoparticles

2.6.1. Physical characterization. The zeta potential was recorded using a Zetaplus instrument and dynamic light scattering (DLS) was used to study the particle size and the

polydispersity index (PI). The stability of the particles was analyzed by noting the size and PI after 20 days. The surface morphology and structure of the nanoparticles were analyzed using SEM images recorded at 5 kV. The nanoparticles were dispersed in distilled water and dropped on a glass cover slip. The cover slip was dried in a desiccator for 3 days to evaporate the solvent, then it was sputter-coated with gold before recording images using the microscope.

2.6.2. Chemical characterization. ^{1}H NMR and ^{13}C NMR spectroscopies were performed to confirm the structure of PGS. FTIR spectroscopy[28] was employed to determine the functional groups present in the nanoparticle and polymer. The lyophilized samples were mixed with potassium bromide (KBr) and pellets were formed using a hydraulic press. Then, the pellets were placed in the FTIR instrument and the spectra were recorded and analyzed. XRD was performed to ensure encapsulation of 5FU within PGS-NP.[22] The thermal stability of PGS was assessed using TGA, and DSC was used to characterize the thermal phase transitions.[29] The averaged molecular weight (M_w) and the number average molecular weight (M_n) of the PGS polymer were calculated using gel permeation chromatography (GPC) analysis in a styragel column using polystyrene standards as reference controls for calculating M_w.

2.7. Drug release study

The dialysis method was used to determine the concentration of 5FU in PBS and, thus, the drug release pattern of the nanoparticles.[30] PGS-5FU NPs were dispersed in PBS and put in a dialysis tube in a beaker with 200 mL of PBS. Every hour, 3 mL of PBS was replaced with fresh PBS in the beaker with stirring at 50 rpm and this was done for 24 h. The drug release rate was obtained by taking readings of the 3 mL of extracted PBS using UV/visible spectroscopy. DD Solver software was used to simulate the drug release kinetics.

2.8. Cellular uptake of the NPs

The nanoparticles were loaded with rhodamine B (0.5 mg mg^{-1} w/w)[31] and the uptake of the NPs was observed using a fluorescence microscope. Around 25 000 cells (MDA-MB-231 and A549) were seeded in separate 60 mm dishes then treated with the rhodamine B loaded nanoparticles. After 12 h of incubation, the cells were washed with PBS and the nucleus was stained with 2 μL of live Hoescht (25 mg mL^{-1}) for 15 min. Images were then taken using a fluorescence microscope (Ti Eclipse Nikon, U.S.A.).

2.9. *In vitro* cytotoxicity study

Cells were seeded in a 96 well plate (5000 cells per well) and, 24 h later, the free drug, PGS nanoparticles and the drug loaded nanoparticles were added to the wells in triplicate at different concentrations; untreated cells were also used in the experiment.[32] Readings were taken at different time points such as 12 h, 24 h, 36 h and 48 h. An MTT stock solution was prepared (5 mg mL^{-1}) and 10 μL was added to each well along with blanks at each time point. 2 h later, the stop solution (DMSO) was added to solubilize the crystals formed. The reading of the samples was performed at 560 nm using an ELISA plate reader (PerkinElmer). The cell viability percentage[33] was calculated using the following formula:

$$\text{Cell viability}\% = \frac{(\text{Mean absorbance of sample} - \text{absorbance of the blank}) \times 100}{\text{Mean of absorbance of the control sample}}$$

2.10. Apoptosis analysis using flow cytometry

The cells were treated for 24 h with free 5FU, PGS-NP, and PGS-5FU and 2×10^5 cells were taken along with the untreated control cells. 50 μL of binding buffer was added to each tube and then annexin V-FITC (5 μL) was added with 10 μL of propidium iodide (PI).[34] After 10 min of incubation at 37 °C, the cells were run through a FACS Calibur instrument to calculate the number of cells undergoing apoptosis. The gating was done using unstained control cells.

2.11. Evaluation of apoptosis

The intrinsic apoptosis pathway is initiated by cleavage of caspase-9, and the cleaved caspase-9 cleaves caspase-3. This cleaved caspase-3 then translocates into the nucleus to induce apoptosis. To understand the mechanism of the NP induced apoptosis, a caspase-3 colorimetric assay kit was used.[35] The protocol given by Takara Bio was followed whereby 2×10^6 treated and control cells were centrifuged at 400*g* for 5 min. Then, 50 μL of cold lysis buffer was added and the solution was kept in ice for 10 min. The tubes were then centrifuged at 12 000*g* for 10 min at 4 °C and the supernatant was transferred to new tubes. One set of positive control cells was treated with 1 μL of caspase-3 inhibitor and 50 μL of reaction buffer containing DTT. The rest of the samples were treated only with reaction buffer having DTT and the solution was incubated for 30 min in ice. Then, 5 μL of the 1 mM caspase-3 substrate was added and kept for 1 h in a water bath at 37 °C. A standard curve was plotted using pNA provided in the kit dissolved in DMSO at different concentrations ranging from 0 to 200 μM.

2.12. Expression levels of apoptosis proteins

MDA-MB-231 cells and A549 cells were treated with 5FU, PGS nanoparticles and PGS-5FU, the cells were trypsinized, and the

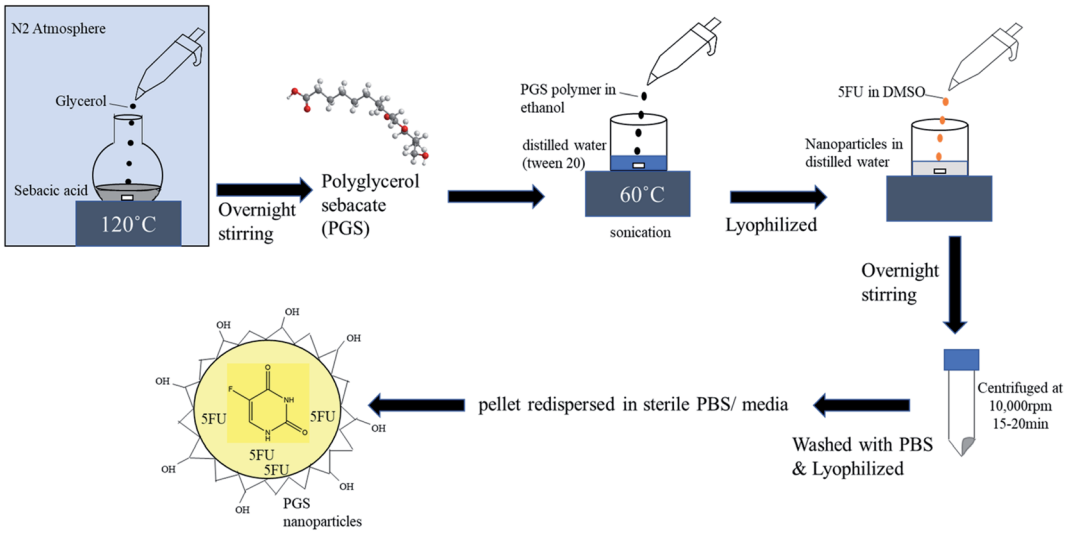

Scheme 1

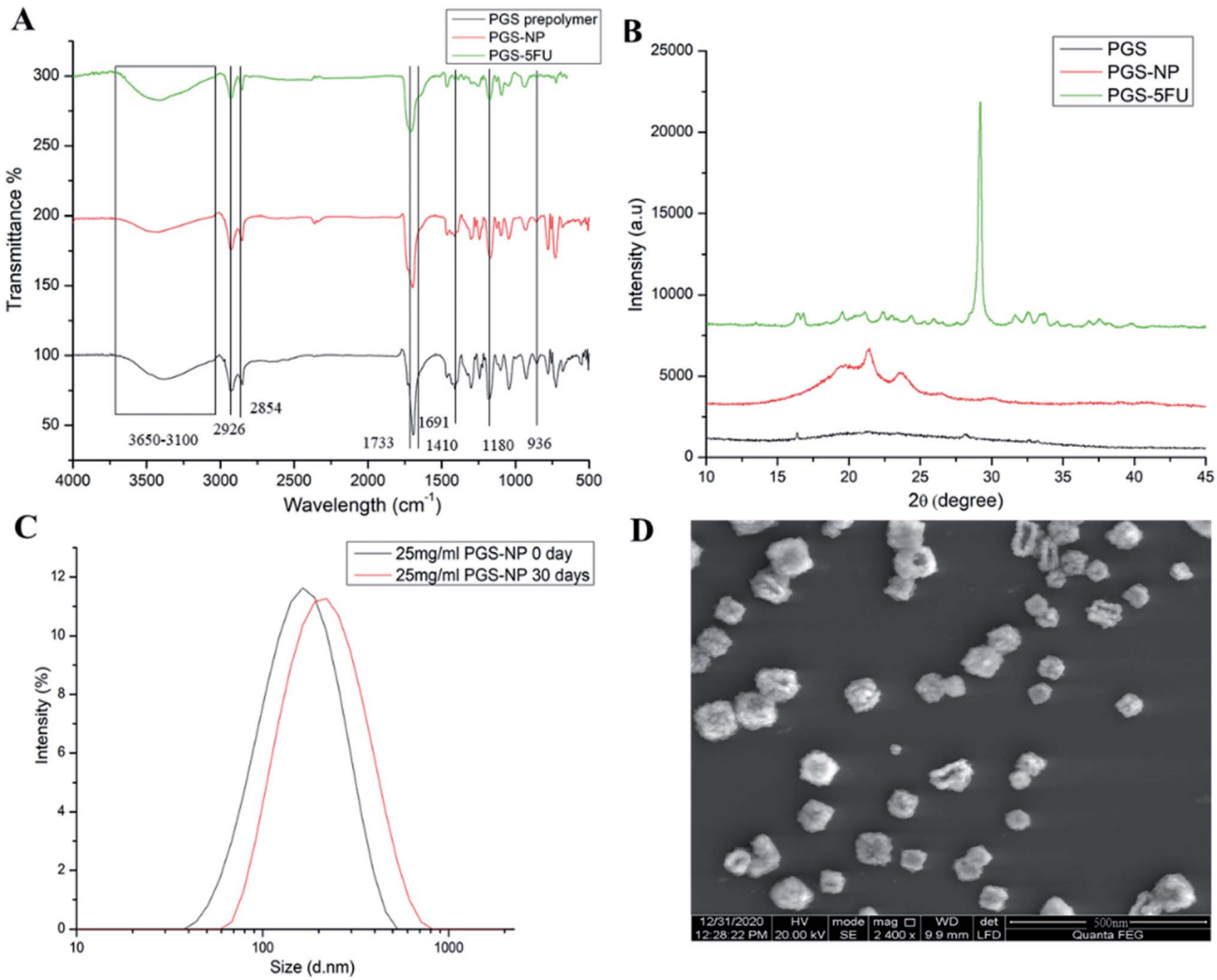

Fig. 1 (A) FTIR spectra of the polyglycerol sebacate prepolymer, PGS nanoparticle and 5FU loaded PGS nanoparticle. (B) Powder XRD analysis of the PGS polymer, PGS nanoparticle and 5FU encapsulated nanoparticle. (C) Dynamic light scattering (DLS) histogram showing a unimodal peak indicating uniformly sized particles; the same was validated using scanning electron microscopy (SEM) (D).

pellets were washed with PBS. The supernatant was discarded, and the total protein was extracted using a radioimmunoprecipitation buffer (RIPA) with a 1× protein inhibition cocktail (PIC).[36] 30 μg of protein of each sample was run using SDS-PAGE and then transferred onto a polyvinylidene difluoride membrane after activation. This membrane was blocked with 5% skimmed milk and then incubated overnight at 4 °C with primary antibodies against procaspase-3, procaspase-9, and vinculin. The membrane was washed with TBS—T thrice and incubated with the respective alkaline phosphatase-conjugated secondary antibody. The blots were developed using an enhanced chemiluminescence (ECL) buffer, imaged using a BioRad ChemiDoc system and analysed by normalizing with an endogenous control vinculin protein.

2.13. Statistical analysis

The statistical data analysis was performed using Student's *t*-test to compare the different samples where $p < 0.05$ was taken to be significant. All the experiments were done in triplicate, the average was noted, and the standard error was plotted using Graphpad Prism 8. Origin Pro 8.5 software was used to plot graphs of FTIR, XRD, and TGA data. Flowjo v8 was used to plot the dot plot of flow cytometry experiments. Image Lab and Fiji ImageJ software were used to analyse western blot and fluorescence microscope images, respectively. To calculate the loading efficiency and the drug release rate, the supply of 5FU was measured over a range of different concentrations and λ_{max} was determined by UV-vis spectroscopy.

3. Results and discussion

3.1. Synthesis and properties of 5FU-NPs

The synthesis of the polyglycerol polymer was done according to a previously reported protocol by taking equimolar amounts of glycerol and sebacic acid, as shown in Scheme 1. The characterization of the monomers and the pure polymer was performed using ^{1}H NMR spectroscopy and data were analyzed using MestReNova software (Fig. S1†). The proton peaks at δ 1.30, 1.60, and 2.3 ppm in the polymer data corresponded to sebacic acid and the peaks at 3.43–3.96, 4.08–4.35, and 5.09, 5.26 ppm are related to glycerol. These data showed a linear structure of the PGS polymer with the molar ratio of monomers of 1. Additionally, this result was corroborated by FTIR analysis (Fig. 1A), which exhibited a broad peak at 3443 cm^{-1} attributed to the stretch vibration absorption of O–H end groups in the molecules while their bending gave a peak at 1410 cm^{-1}. The sharp peaks at 1180 cm^{-1} and 1733 cm^{-1} are related to C–O whereby the 1733 cm^{-1} peak indicated an ester carbonyl linkage. C═O bonds and methylene groups were indicated by peaks at 2854 cm^{-1} and 2926 cm^{-1}, respectively. The peak at 1691 cm^{-1} indicates unreacted sebacic acid and this peak was absent in the spectrum of the polymer owing to the purification step. These data demonstrate the successful generation of the PGS polymer and the active groups on the surface can be functionalized further to attach compounds onto the surface of the nanoparticles. XRD analysis (Fig. 1B) showed a sharp peak in the pattern of the PGS-5FU nanoparticles at 30 2θ and a peak at 20 2θ present in the pattern of

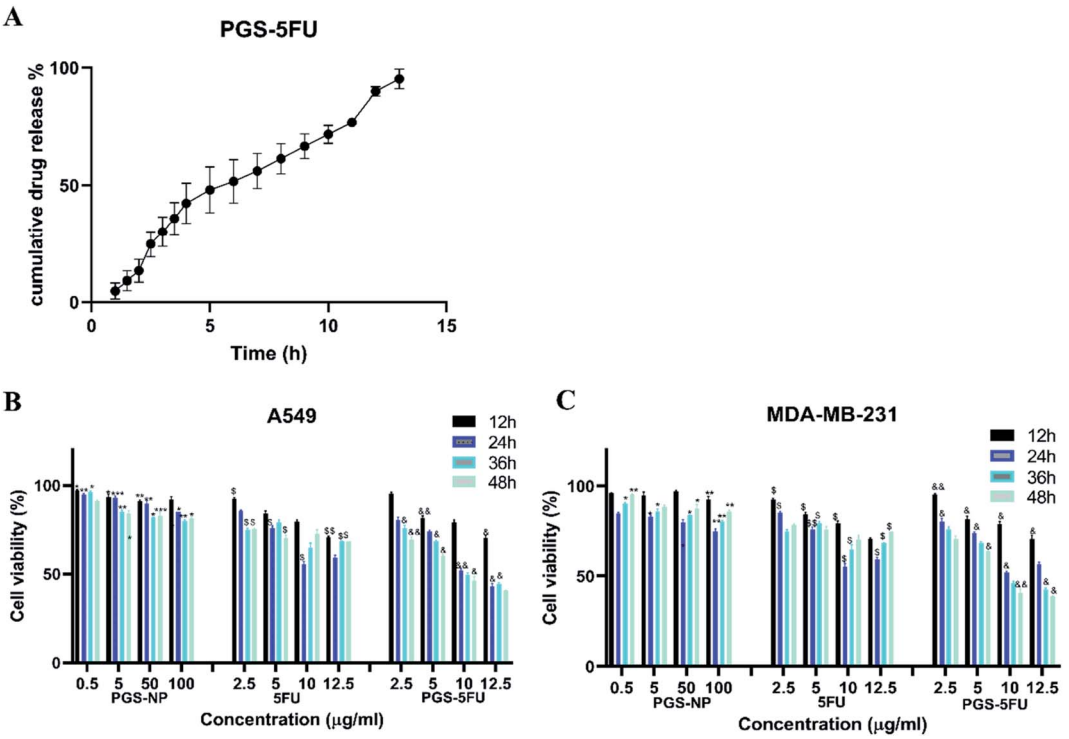

Fig. 2 (A) Cumulative release rate of 5FU from the drug loaded NPs. (B and C) Cytotoxicity assay with different concentrations of PGS-NP, 5FU and PGS-5FU done with A549 and MDA-MB-231 cells, respectively (*$p < 0.05$ *vs.* PGS-NP, $p < 0.05$ *vs.* 5FU, &$p < 0.05$ *vs.* PGS-5FU).

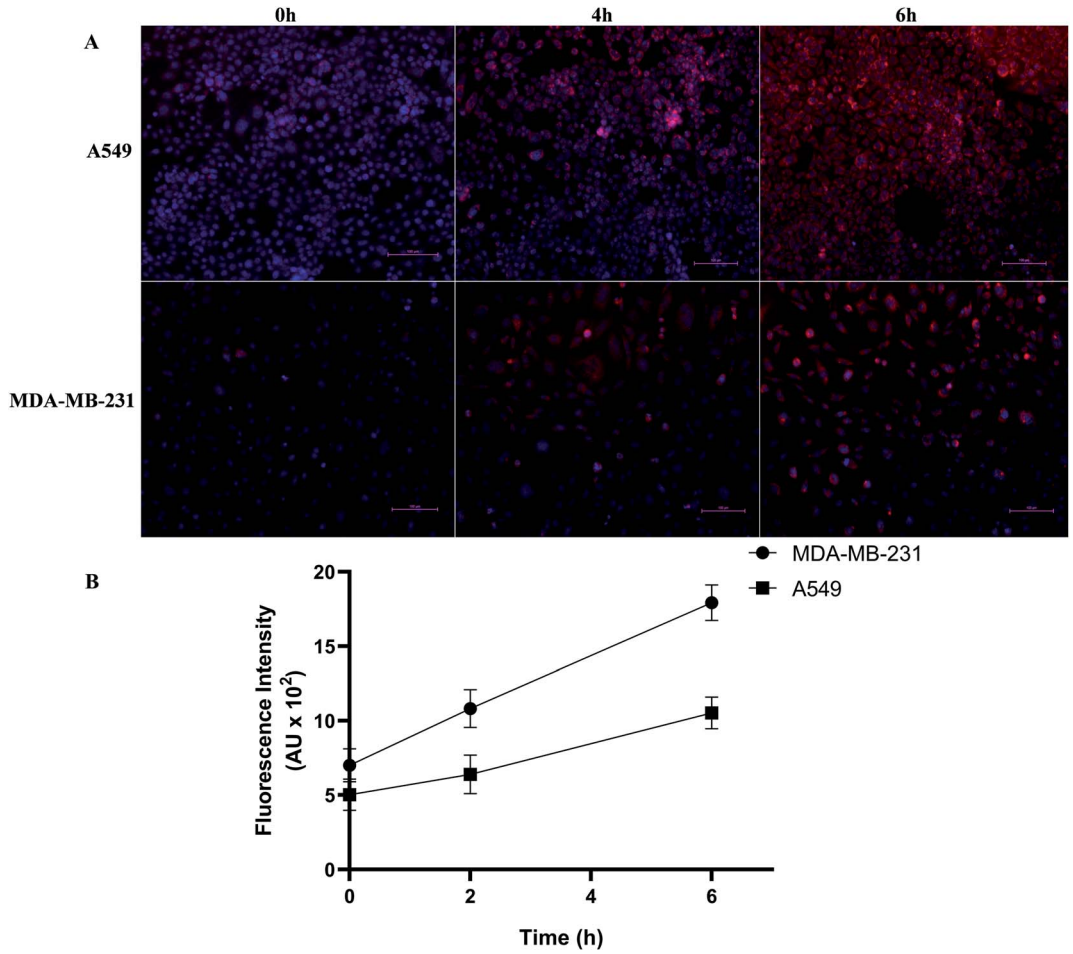

Fig. 3 (A) Increasing uptake of Rho-NPs by A549 as well as MDA-MB-231 cells with time and (B) its quantified representation.

PGS-NP that had almost completely disappeared in the pattern of PGS-5FU, showing the encapsulation of 5FU within PGS-5FU. These data confirm the crystalline nature of the nanoparticles as compared to the semi-crystalline nature of the PGS gel and, therefore, the increased stability of PGS-5FU. The thermostability of PGS-NP and PGS-5FU was assessed using a thermogravimetric analyzer (TGA-Q50) and a representative thermogram is plotted in Fig. S2.† The results showed a first weight loss of about 30% at 250 °C for the PGS nanoparticles and a second thermal decomposition at 400 °C of 40% weight loss. The first weight loss is due to absorbed solvent evaporation and the second one is due to polymer degradation. In the case of the 5FU loaded PGS nanoparticles, there was a weight loss of up to 90% in the range from 300 °C to 400 °C, indicating an increase in stability with the encapsulation of 5FU. The heat flow through the PGS prepolymer, PGS-NP and PGS-5FU was measured by differential scanning calorimetry (DSC Q200, TA Instruments) (Fig. S3†). The results showed a glass transition temperature (T_g) of the PGS prepolymer of −7.52 °C and that of PGS-NP of 104.87 °C. The shift to positive temperature is due to the increased crosslinking within the nanoparticle. Additionally, the melting temperature (T_m) was 5.56 °C for the PGS prepolymer, which increased to 105.33 °C for PGS-NP, indicating that PGS is miscible with the sol–gel composite and that the nanoparticle has partial crystallinity. Interestingly, after loading 5FU into the nanoparticle, it became completely amorphous, and this suggests the successful entrapment of the drug within the nanoparticle matrix. Furthermore, GPC analysis (GPC, Waters, U.S.A.) showed a PDI of the PGS polymer of 1.0054, a calculated M_n of 93.9 kDa and a M_w of 94.4 kDa using polystyrene standards for generating the calibration curve.

3.2. Morphological characteristics of the nanoparticle

The size and zeta potential of the nanoparticles were assessed using a Malvern Instruments Zetasizer nano ZS90. The size distribution histogram (Fig. S5†) showed varied sizes for different concentrations of PGS used to make the nanoparticles. Interestingly, the size and PDI data for the 25 mg mL^{-1} concentration of PGS measured 30 days post synthesis showed homogenous particles in the range of 200–350 nm and having long shelf-life stability (Fig. 1C). The observed zeta potential was between −35 mV and −20 mV. The zeta potential magnitude of PGS-NPs indicates high colloidal stability. These nanoparticles are also small-sized, within which the drug can be easily loaded. To corroborate the results, scanning electron microscopy (SEM)

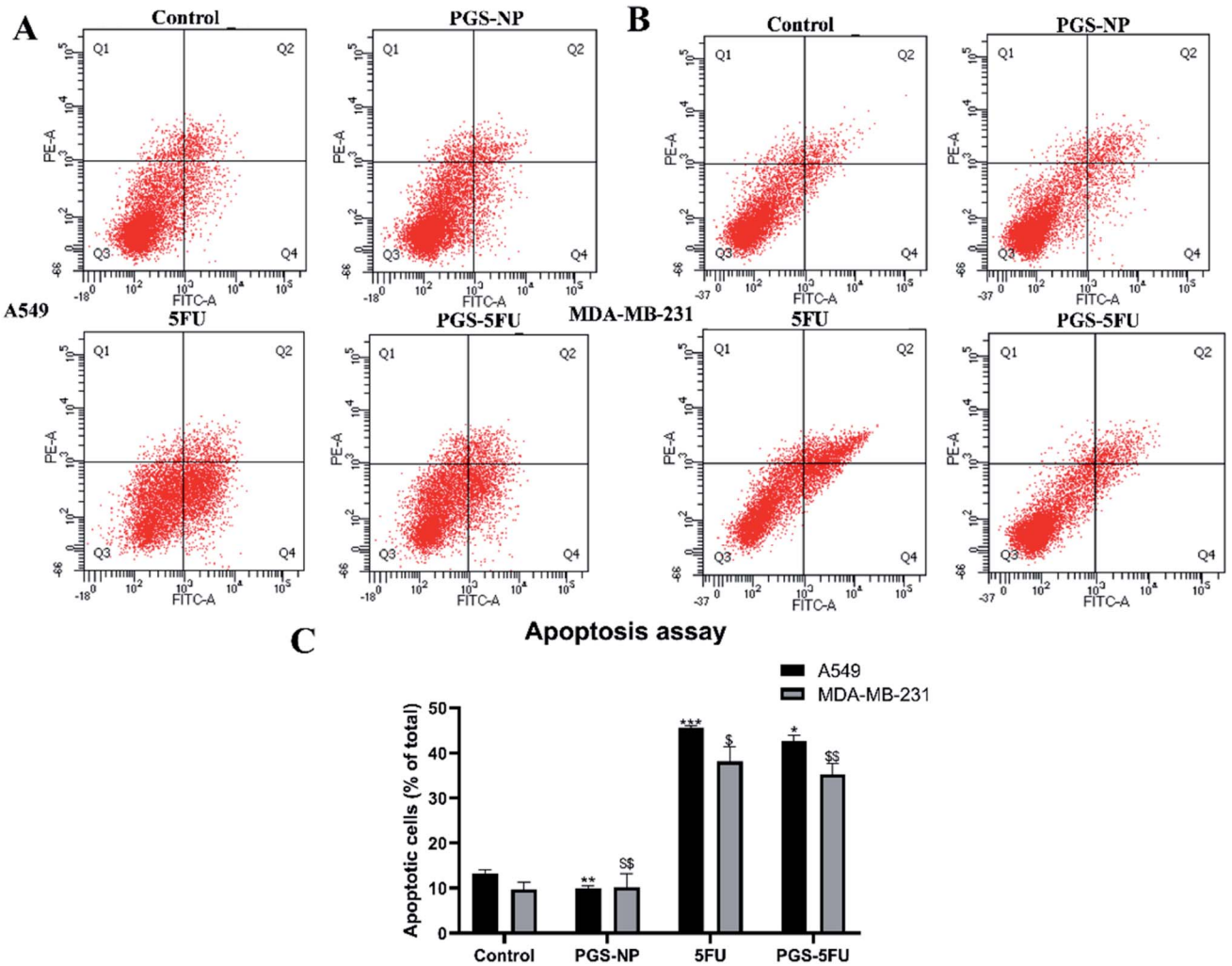

Fig. 4 (A and B) Dot plot of Annexin V-FITC assay performed with A549 cells and MDA-MB-231 cells, respectively. A quantitative histogram of the apoptotic cell population present in each sample is plotted below (C) (*p < 0.05 *vs.* A549 control group, $$p$ < 0.05 *vs.* MDA-MB-231 control group).

(Fig. 1D) was used, which exhibited PGS nanoparticles having a spherical shape.

3.3. *In vitro* 5FU release kinetics

The loading efficiency of different nanoparticle to drug ratios was calculated and, out of these, the 1 : 2.5 ratio of PGS-NP : 5FU showed a 90.39% encapsulation efficiency. Additionally, the release of 5FU *via* diffusion recorded over 15 h showed a controlled drug release (Fig. 2A). A graph was plotted of the drug release rate and, at 13 h, almost all of the loaded drug was released into the medium. With the help of mathematical modelling using DD Solver software, the kinetics of 5FU-NP was determined to be Hopfenberg with R square calculated as 0.985.

3.3.1. Hopfenberg's erosion-based model. This model indicates surface erosion of the polymeric NPs where a zero-ordered release of the drug is the rate-limiting step. This equation that is valid for cylinders and spheres can be expressed as follows:

$$\frac{M_t}{M_\infty} = 1 - \left(1 - \frac{k_0 \times t}{c_0 \times a}\right)^n$$

where M_t and M_∞ are the cumulative amounts of drug released at time t and infinity; k_0 is the erosion rate constant; c_0 is the amount of drug loaded in the NPs; a is the radius of the spherical NP and n is the shape factor, which is 3 for spheres.

This kinetic model suggests a controlled release from a spherical matrix such that the PGS nanoparticles retain their shape and properties in PBS with the slow degradation of the NPs. This is advantageous as the ideal biodegradable NPs must degrade at the tumor site while releasing the drug in a controlled manner.

3.4. Cytotoxic effect of PGS-5FU

Stock solutions of different concentrations of PGS were prepared in distilled water and then working concentrations were diluted in biological media. At different time points, the absorbance was recorded after solubilizing crystals formed due

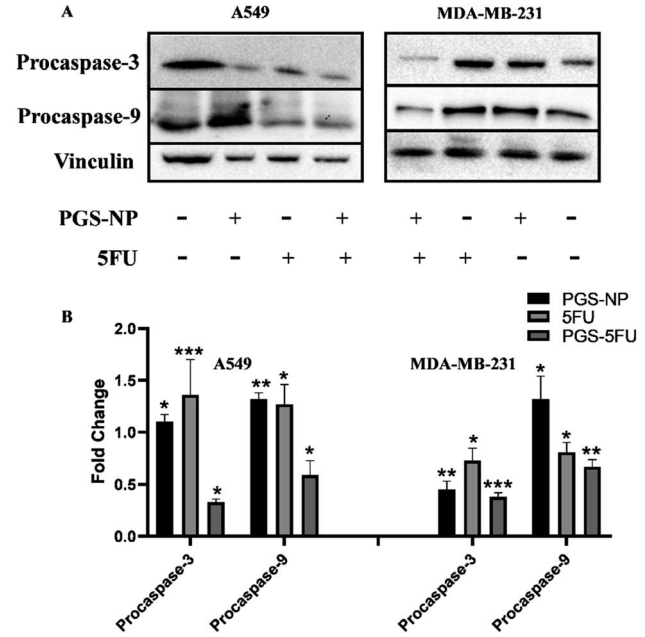

Fig. 5 (A) Western blots showing expression levels of inactive proteases caspase-3 and caspase-9 when A549 and MDA-MB-231 cells were treated with PGS-NP, 5FU and PGS-5FU, respectively. (B) Histogram representation with quantitative analysis of the blots.

to the addition of MTT, and the cell viability percentage was calculated (Fig. 2B and C). Interestingly, even at higher concentrations of PGS-NPs, there was no significant decrease in cell viability up to 48 h. This could illustrate the biocompatibility of the polymeric PGS nanoparticles. The 50% inhibitory concentration (IC_{50}) of 5FU was calculated as 10.86 ± 0.34 μg mL^{-1} for A549 cells and 11.18 ± 0.42 μg mL^{-1} for MDA-MB-231 cells. Furthermore, PGS-5FU had IC_{50} values in similar ranges, calculated as 10.49 + 0.22 μg mL^{-1} (A549) and 10.88 + 0.17 μg mL^{-1} (MDA-MB-231). But, after 24 h, 36 h, and 48 h, the viability% increased when cells were treated with the drug alone, demonstrating that the cells became resistant and survived. Interestingly, the cell viability decreased with time upon treatment with PGS-5FU nanoparticles. This clearly shows the improved efficiency of PGS-5FU nanoparticles in the controlled release of 5FU as compared to 5FU alone. Therefore, this drug delivery system can enhance the competence of existing conventional chemotherapy and help avoid resistance development and metastasis of the disease.

3.5. Cellular uptake of PGS-5FU nanoparticles

The fluorescent dye rhodamine B was encapsulated in the PGS-NPs (Rho-NPs) to understand the efficiency of uptake of the nanoparticles by cancer cells. There was a gradual increase in the fluorescence with time (Fig. 3). At 6 h, almost all the cells showed the intracellular uptake of Rho-NPs. The images showed that the NPs were transported efficiently into the cells. One of the key requisites of a drug delivery system is the ability of the nanoparticle to penetrate the cell membrane; here, it can be seen that these PGS-NPs loaded with rhodamine were easily taken up by the

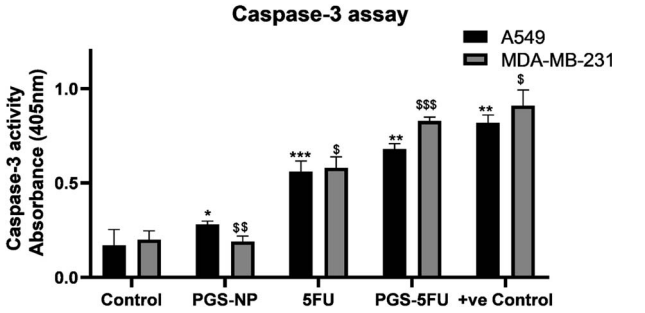

Fig. 6 Increasing activity of caspase-3 protease when cells were treated with PGS-5FU in both cell lines (*p < 0.05 *vs.* A549 control group, \$$p$ < 0.05 *vs.* MDA-MB-231 control group).

cancer cells. Within a few hours, the nanoparticles were internalized in the cancer cells and, therefore, PGS-NPs could deliver the anti-cancer drugs enclosed within them inside the cells.

3.6. Apoptosis assay using flow cytometry

To estimate the induction of apoptosis upon treatment with the drug loaded nanoparticles, Annexin V-FITC assay was performed wherein the treated cells along with control cells were stained with propidium iodide and Annexin V-FITC dyes. Calibration gating was performed using unstained cells, and results were obtained using flow cytometry (Fig. 4). The dot plots validated that PGS-5FU treatment induced apoptosis in the cancer cells as there was a shift seen towards the Q2 and Q4 quadrants, as shown in Fig. 4A and B, indicating late and early apoptosis, respectively. A549, as well as MDA-MB-231 cells treated with PGS-NPs had lower populations in these quadrants, which confirms the previous toxicity findings. These outcomes provide insight into the molecular mechanism of PGS-5FU nanoparticles and confirm that the cell death is caused by apoptosis induction.

3.7. Immunoprecipitation analysis of apoptotic proteins

The western blot analysis (Fig. 5) also indicated cell death *via* apoptosis for the cells treated with PGS-5FU nanoparticles. To prove the same, the expression levels of inactive caspase-3 and caspase-9 proteins were recorded, and they remained almost the same when normalized with vinculin protein in the case of PGS-NP and 5FU treatment in A549 cells. This means that neither the PGS nanoparticles nor 5FU alone could initiate apoptosis in the cancer cells. However, there was a significant decrease in the protease levels upon treatment with PGS-5FU, evidently showing initiation. In MDA-MB-231 cells as well, a similar pattern of expression levels was observed. The significant downregulation of procaspases in both cell lines when treated with the drug loaded nanoparticles proves the augmented ability of PGS-5FU nanoparticles in initiating apoptosis in cancer cells.

3.8. Caspase-3 assay

When initiating apoptosis, caspase proteases play a very crucial role. The activity of caspase-3 indicates the process of apoptosis and, therefore, to assess the effect of PGS-5FU, colorimetric

caspase-3 assay was performed. The protease levels of the A549 lung cancer and MDA-MB-231 breast cancer cells treated with PGS-5FU at the IC_{50} concentration were different (Fig. 6). The breast cancer cells showed a 4.15-fold change in caspase-3 levels and the A549 cells showed a 4-fold change in levels, but the 5FU treated MDA-MB-231 cells, and A549 cells showed 2.9- and 3.29-fold changes of caspase-3 levels, respectively. This is due to the different cellular uptake rates of PGS-5FU within these two cell lines in the given period and also indicates that breast cancer cells are more sensitive to PGS-5FU treatment. As mentioned earlier, PGS-NPs did not initiate apoptosis as the caspase-3 levels were significantly low as compared to the untreated control cells.

4. Conclusion

A polymeric polyglycerol sebacate nanoparticle was synthesized and successfully loaded with 5FU. The hydroxyl functional groups present on the PGS polymer make it hydrophilic,[37] and the MTT assay showed that PGS-NPs, even at higher concentrations like 100 μg mL^{-1}, did not have a toxic effect on cancer cells, thus making them biocompatible. Characterization of the generated PGS-NPs illustrated uniformly sized, spherical particles (200–350 nm) that were highly stable over an extended period of 30 days. Additionally, this PGS nanoparticle was easily taken up by the cancer cells within 6 h, proving it to be an efficient vehicle for internalization of the drug within cancer cells. The PGS-5FU nanoparticles showed a sustained low cell viability percentage for over 48 h whereas the free drug showed an increased cell viability post 24 h in both the lung cancer and breast cancer cells with calculated IC_{50} values of 10.49 ± 0.22 μg mL^{-1} and 10.88 ± 0.18 μg mL^{-1}, respectively. The PGS-5FU nanoparticles exhibited a controlled drug release property that prevented resistance development and eliminated cancer cells. To corroborate this, apoptosis assay was performed using flow cytometry, and the data indicated the ameliorated potential of the PGS-5FU nanoparticles to cause apoptosis in A549 and MDA-MB-231 cells when compared to PGS-NP or 5FU treatment. Also, the PGS-5FU nanoparticles showed an almost 3 times increase in caspase-3 activity upon treatment as compared to control cells. These PGS-5FU nanoparticles exhibited improved properties over some popular polymeric nanoparticles like PEGylated PLGA nanoparticles[38] and chitosan nanoparticles,[39] which have reported 5FU encapsulation efficiencies of 80.37 and 69.69% whereas, in the current study, PGS-5FU nanoparticles had an efficiency of 90.39%. In another article, PGS was chemically conjugated with a derivative of 5FU;[40] however, in the present case, 5FU is encapsulated within PGS nanoparticles, making their synthesis very easy. Thus, this delivery system is much more efficient and can more easily generate 5FU loaded nanoparticles. In conclusion, this study reports a novel polymeric PGS nanoparticle as an excellent drug delivery system to improve the solubility of anti-cancer drugs with enhanced biocompatibility. It can also increase the efficiency of the traditional chemotherapy to provide a better quality of life for cancer patients.

Conflicts of interest

There is no conflict of interests to declare.

Acknowledgements

The authors are thankful for the timely and crucial suggestions given by Dr Ramya Kannan and the help with the design of the work. Ms Alphy Sebastian and Ms Swatilekha were supportive and patient in helping with the working of instruments. The authors heartfully thank Mr Rakiraj from the Metallurgy and Mechanical Engineering Department, IIT Madras for taking precise SEM images. D. S. wants to thank Mr Bamadeb for carrying out flow cytometry experiments and helping with the analysis.

References

1 World Health Organization, *WHO reports*, 2018, pp. 6–13.
2 World Health Organization, *Key facts*, https://www.who.int/news-room/fact-sheets/detail/cancer.
3 R. L. Siegel, K. D. Miller and A. Jemal, *Ca-Cancer J. Clin.*, 2020, **70**, 7–30.
4 A. S. B. Primeau, *Cancer Recurrence Statistics*, Cancer Therapy Advisor, 2018, 1–9.
5 H. Sung, J. Ferlay, R. L. Siegel, M. Laversanne, I. Soerjomataram, A. Jemal and F. Bray, *Ca-Cancer J. Clin.*, 2021, 1–41.
6 National Cancer Institute, *Types of Cancer Treatment*, NIH, 2015, pp. 1–4.
7 D. B. Longley, D. P. Harkin and P. G. Johnston, *Nat. Rev. Cancer*, 2003, **3**, 330–338.
8 H. Kato, Y. Ichinose, M. Ohta, E. Hata, N. Tsubota, H. Tada, Y. Watanabe, H. Wada, M. Tsuboi, N. Hamajima and M. Ohta, *N. Engl. J. Med.*, 2004, 1713–1721.
9 J. Nakano, C. Huang, D. Liu, D. Masuya, T. Nakashima, H. Yokomise, M. Ueno, H. Wada and M. Fukushima, *Br. J. Cancer*, 2006, **95**, 607–615.
10 D. A. Cameron, H. Gabra and R. C. F. Leonard, *Br. J. Cancer*, 1994, **70**, 120–124.
11 C. J. Creel, M. A. Lovich and E. R. Edelman, *Circ. Res.*, 2000, **86**, 879–884.
12 D. Bobo, K. J. Robinson, J. Islam, K. J. Thurecht and S. R. Corrie, *Pharm. Res.*, 2016, **33**, 2373–2387.
13 A. C. Anselmo and S. Mitragotri, *Bioeng. Transl. Med.*, 2019, **4**, 1–16.
14 G. Pillai, *SOJ Pharm. Pharm. Sci.*, 2014, **1**(2), 13.
15 S. Sawant and R. Shegokar, *Int. J. Canc. Ther. Oncol.*, 2014, **2**, 020408.
16 D. J. Adams, *Trends Pharmacol. Sci.*, 2012, **33**, 173–180.
17 L. Di, P. V. Fish and T. Mano, *Drug Discovery Today*, 2012, **17**, 486–495.
18 K. W. Lee and Y. Wang, *J. Visualized Exp.*, 2011, 1–6.
19 X. Zhang, C. Jia, X. Qiao, T. Liu and K. Sun, *Polym. Test.*, 2016, **54**, 118–125.
20 B. Xiao, W. Yang, D. Lei, J. Huang, Y. Yin, Y. Zhu, Z. You, F. Wang and S. Sun, *Adv. Healthcare Mater.*, 2019, **8**, 1–14.

21 Y. Wang, H. Wu, Z. Wang, J. Zhang, J. Zhu, Y. Ma, Z. Yang and Y. Yuan, *Polymers*, 2019, **11**(6), 965, DOI: 10.3390/polym11060965.
22 B. Louage, L. Tack, Y. Wang and B. G. De Geest, *Polym. Chem.*, 2017, **8**, 5033–5038.
23 N. Zanjanizadeh Ezazi, R. Ajdary, A. Correia, E. Mäkilä, J. Salonen, M. Kemell, J. Hirvonen, O. J. Rojas, H. J. Ruskoaho and H. A. Santos, *ACS Appl. Mater. Interfaces*, 2020, **12**, 6899–6909.
24 C. P. Dora, S. K. Singh, S. Kumar, A. K. Datusalia and A. Deep, *Acta Pol. Pharm.*, 2010, **67**, 283–290.
25 Y. Jia, W. Wang, X. Zhou, W. Nie, L. Chen and C. He, *Polym. Chem.*, 2016, **7**, 2553–2564.
26 A. Pourjavadi, S. S. Amin and S. H. Hosseini, *Ind. Eng. Chem. Res.*, 2018, **57**, 822–832.
27 D. Press, *Int. J. Nanomed.*, 2017, 4085–4109.
28 A. Saudi, M. Rafienia, A. Zargar Kharazi, H. Salehi, A. Zarrabi and M. Karevan, *Polym. Adv. Technol.*, 2019, **30**, 1427–1440.
29 B. C. Tang, C. L. Yao, K. Y. Xieh and S. G. Hong, *J. Polym. Res.*, 2017, **24**, 1–8.
30 X. Li, L. Li, Y. Huang, B. Liu, H. Chi, L. Shi, W. Zhang, G. Li, Y. Niu and X. Zhu, *Biomater. Sci.*, 2017, **5**, 2068–2078.
31 A. Jonderian and R. Maalouf, *Front. Pharmacol.*, 2016, **7**, 1–7.
32 E. Lee, H. Jeon, M. Lee, J. Ryu, C. Kang, S. Kim, J. Jung and Y. Kwon, *Sci. Rep.*, 2019, **9**, 1–13.
33 C. M. Park and M. Xian, *Methods Enzymol.*, 2015, **554**, 127–142.
34 X. Lu, J. Qian, H. Zhou, Q. Gan, W. Tang, J. Lu, Y. Yuan and C. Liu, *Int. J. Nanomed.*, 2011, **6**, 1889–1901.
35 Y. Pan, M. Guo, Z. Nie, Y. Huang, Y. Peng, A. Liu, M. Qing and S. Yao, *Chem. Commun.*, 2012, **48**, 997–999.
36 R. P. Arun, D. Sivanesan, B. Patra, S. Varadaraj and R. S. Verma, *Sci. Rep.*, 2019, **9**, 1–12.
37 P. Denis, M. Wrzecionek, A. Gadomska-Gajadhur and P. Sajkiewicz, *Polymers*, 2019, **11**(12), 2113.
38 Y. A. Haggag, M. A. Osman, S. A. El-Gizawy, A. E. Goda, M. M. Shamloula, A. M. Faheem and P. A. McCarron, *Biomed. Pharmacother.*, 2018, **105**, 215–224.
39 R. S. Tiğli Aydin and M. Pulat, *J. Nanomater.*, 2012, 42.
40 Z. J. Sun, B. Sun, C. W. Sun, L. B. Wang, X. Xie, W. C. Ma, X. L. Lu and D. L. Dong, *J. Bioact. Compat. Polym.*, 2012, **27**, 18–30.